Project	IEEE P802.15 Working Group for Wireless Personal Area Networks (WPANs)		
Title	**The Ultra-Wide Bandwidth Indoor Channel: from Statistical Model to Simulations**		
Date Submitted	["24 June, 2002"]		
Source	[Moe Z. Win] [Allcomms Consulting] []	Voice: Fax: E-mail:	[ ] [ ] [win@ieee.org]
Source	[Dajana Cassioli] [RadioLabs] [via del Politecnico, 1 00133 Rome - ITALY]	Voice: Fax: E-mail:	[+39 06 7259 7439] [+39 06 7259 7435] [cassioli@radiolabs.it]
Source	[Andreas F. Molisch] [MERL Mitsubishi Electric Research Laboratory, Murray Hill] [571 Central Avenue, Murray Hill, NJ]	Voice: Fax: E-mail:	[+ 1 908 363 0524] [+ 1 908 665 2414] [Andreas.Molisch@ieee.org]
Re:	[Response to Call for Contributions on Ultra-wideband Channel Models, Doc. IEEE P802.15-02/208r1-SG3a.]		
Abstract	We propose a statistical model for the ultra-wide bandwidth (UWB) indoor channel based on an extensive measurement campaign in a typical modern office building. Our model is formulated as a stochastic tapped-delay-line (STDL) model of the UWB indoor channel. The averaged power delay profile is modeled by a single exponential decay with a statistically distributed decay constant. The small-scale statistics of path gains follow Gamma distributions whose parameters *m* are truncated Gaussian variables with mean values and standard deviations decreasing with delay. The total received energy experiences a lognormal shadowing around the mean energy given by the path-loss law. The fading of the taps is uncorrelated. Finally, we propose an implementation of the STDL model.		
Purpose	[Submission to P802.15 for the standardization of an indoor UWB channel model]		
Notice	This document has been prepared to assist the IEEE P802.15. It is offered as a basis for discussion and is not binding on the contributing individual(s) or organization(s). The material in this document is subject to change in form and content after further study. The contributor(s) reserve(s) the right to add, amend or withdraw material contained herein.		

Dajana Cassioli†, Student Member, IEEE, Moe Z. Win, Senior Member,IEEE, and Andreas F. Molisch, Senior Member, IEEE

I. INTRODUCTION

Scope: Ultra-wide bandwidth (UWB) spread-spectrum techniques have recently attracted great interest in scientific, commercial, and military sectors, so that the UWB systems are considered as possible candidates for an alternative PHY for the IEEE 802.15 study group 3a. In order to test and compare various physical-layer schemes suggested for this standard, a channel model is required. For this reason, IEEE802.15 has called for suggestions for channel models in three areas: 1) path loss; 2) fading statistics; and 3) interference. While the FCC notice allows both for outdoor peer-to-peer, and for indoor communications, the main interest of the research community lies in the latter one. In this document, we propose a comprehensive indoor channel model for the *fading statistics* of the UWB channel, covering the second point in the call for

Dajana Cassioli†, Student Member, IEEE, Moe Z. Win, Senior Member,IEEE, and Andreas F. Molisch, Senior Member, IEEE

contributions. We also stress that our model can be easily combined with field-strength and interference models to give a comprehensive channel model for the simulation of complete systems.

We propose a stochastic tapped delay line (STDL) propagation model for the UWB indoor channel. The proposed model is suitable for implementation of computer simulations of a generic UWB system operating in a typical indoor environment. As a matter of fact, simulation programs for tapped delay line channel exist at many research institutions. Furthermore, we would be willing to put our MATLAB simulation program at the disposal of the UWB community, for example by making it downloadable from a website.

All the parameters of the STDL model have been extracted from a set of measured impulse responses, using 2ns-wide baseband pulses. Although the presented parameterization of the model is related to the particular building (indoor residential structures, and large structures like conference halls and airport lounges, might require different parameter settings), and the frequency range in which the propagation experiment was performed, the methodology can be adopted to interpret other similar sets of UWB experimental data. We envisage soon having experimental data in the FCC bands at which we will apply the proposed methodology. We maintain that the parameterization proposed in this document reflects well the properties of typical office buildings. This is also confirmed by extensive literature surveys that show that – in contrast to field strength - the fading parameters vary comparatively little with the center frequency.

Existing models: Many propagation measurements have been performed for indoor narrowband channels and several models have been proposed in the literature [1-4].[1] However, due to their restriction on measurement bandwidth, they are inadequate for the UWB system studies.[1] Even the model in [1] is based on measurements made by probing the channels with only 10 *ns* pulses at 1.5 GHz. In this paper, we present a statistical analysis of the data collected from a UWB propagation experiment, performed in a typical modern office building with 2 nanoseconds delay resolution using baseband pulses [5]. The approach is based on the investigation of the statistical properties of the multipath profiles measured in different rooms over a finely-spaced measurement grid. We analyze this data to arrive at a model for the UWB channel. Our modelling concept is based on well-validated approaches, like the models proposed in [1, 2, 6]. However, some important modifications are made to account for the special properties specific to UWB transmission.

Previous analyses of UWB systems in multipath environments use narrowband channel models or straightforward extensions to finer delay resolutions. For example, [7] uses the model of [1] as well as a deterministic two path model, and [8] uses an extension of the Δ-K model [3,

[1] In mobile radio, it is common to define "narrowband" as transmission bandwidth being much smaller than the coherence bandwidth of the channel. However in this paper, we use the RF engineering definition of narrowband, which is defined as the measurement bandwidth being much smaller than the carrier frequency.

Dajana Cassioli†, Student Member, IEEE, Moe Z. Win, Senior Member,IEEE, and Andreas F. Molisch, Senior Member, IEEE

4, 9] to a delay resolution of 5 nanoseconds. More generally, performance analyses of UWB systems are usually based on channel models that imply Rayleigh fading. However, our analysis shows that the empirical distribution of the path gains markedly differs from the exponential power statistics (i.e., Rayleigh amplitude statistics). This is due to the fact that UWB systems provide high resolution in the delay domain, implying that only a small number of multipath components (MPCs) fall within an interval of delay resolution.[2]

II. MODELING PHILOSOPHY

We separately model the effects of the *large* and *small* scale fading statistics. The large scale fading characterizes the changes in the received signal when the receiver position varies over a significant fraction of the transmitter - receiver (T-R) distance and/or the environment around the receiver changes. This situation typically occurs when the receiver is moved from one room to another room in a building.[3] The small-scale effects, on the other hand, are manifested in the changes of the PDP caused by small changes of the receiver position, while the environment around the receiver does not change significantly. The small-scale statistics can be characterized by investigating the statistical properties of multipath profiles measured over a finely-spaced grid. In the following, we refer to the PDP measured at one specific location as *local* PDP, while we denote the PDP averaged over the locations within one room as the *small-scale averaged* PDP (SSA-PDP). This spatial averaging removes the effect of small scale fading. We also make a distinction between the "local" parameters, which refer to the small-scale effects, and the "global" parameters, describing the changes of the SSA-PDPs. For clarity, all the symbols and parameters are listed in Table I.

TABLE I

SYMBOLS AND PARAMETERS

[2] The resolution of the signal is proportional to the inverse of the bandwidth

[3] More generally speaking, large-scale changes are defined as changes that render the statistical wide-sense stationariy invalid. This means typically changes of more than 20 wavelengths, though the exact number depends on the environment. Thus, there can also be large-scale changes within one room. To simplify notation, in the following we speak of "within a room" when we mean variations over a range where the wide-sense statistical stationarity is fulfilled.

Dajana Cassioli†, Student Member, IEEE, Moe Z. Win, Senior Member,IEEE, and Andreas F. Molisch, Senior Member, IEEE

DELAY AXIS	
τ	Excess Delay
τ_{Ref}	Absolute Propagation Delay
$\tau_k = (k - 1)\Delta\tau$	k^{th} Delay Bin
$\Delta\tau$	Bin Width
N_{bins}	Number of Bins
ENERGY GAINS	
G_{tot}	Total Average Energy Gain
$\overline{G}_k$	Average Energy Gain of the k^{th} Delay Bin
G_k	Energy Gain of the k^{th} Delay Bin
$g(\tau)$	Average Received Energy at Excess Delay τ
EXPONENTIAL TIME DECAY	
ε	Decay Constant
$r = \overline{G}_2 / \overline{G}_1$	Power Ratio

As in any wireless channel, the received signal is a sum of the replicas (echoes) of the transmitted signal, being related to the reflecting, scattering, and/or deflecting objects via which the signal propagates. Each of the echoes is related to a single such object. The received signal may be modeled as a linear combination of N_{path} delayed basic waveforms $w(t)$

$$r(t) = \sum_{i=1}^{N_{path}} c_i w(t - \tau_i) + n(t), \tag{1}$$

where $n(t)$ is the observation noise.

Since the absolute propagation delays of the received signals vary from one location to another, an appropriate delay reference is needed to characterize the relative delays of each resolved MPC. We take the reference τ_{Ref} as the absolute propagation delay, i.e., the delay of the direct or quasi line-of-sight (LOS) path given according to the geometry: $\tau_{Ref} = d/c$, where d is the T-R separation distance and c is the speed of light. We then translate the delay axis of the measured multipath profiles for each location by its respective τ_{Ref}.

As in [2], the delay axis is quantized into bins, and the received power is integrated within each bin to obtain the local PDP in terms of the pairs $\{G_k, \tau_k\}$, where G_k is the energy gain

Dajana Cassioli†, Student Member, IEEE, Moe Z. Win, Senior Member,IEEE, and Andreas F. Molisch, Senior Member, IEEE

defined as the ratio between the energy received at a T-R distance d, over a bin width $\Delta\tau$ beginning at the delay $\tau_k = (k\text{ -}1)\,\Delta\tau$, and the total energy received at the reference distance of one meter.[4]

III. LARGE SCALE STATISTICS

The SSA-PDPs exhibit an exponential decay as a function of the excess delay. Since we perform a delay axis translation, the direct path always falls in the first bin in all the PDPs.[5] The direct path is always the strongest path, even if the line-of-sight is obstructed. The energy of the subsequent MPCs decay exponentially with delay starting from the second bin.

Let $\overline{G}_k = \mathrm{A}_{\mathrm{Spa}}\{G_k\}$ be the locally averaged energy gain, where the $\mathrm{A}_{\mathrm{Spa}}\{\cdot\}$ denotes the spatial average over the region of statistical stationarity. The average energy of the second MPC may be expressed as a fraction r of the average energy of the direct path, i.e. $r = \overline{G}_2/\overline{G}_1$. We refer to r as the *power ratio*. The SSA-PDP is completely characterized by $\overline{G}_1$, the power ratio r, and the decay constant ε (or equivalently, by the total average received energy $\overline{G}_{tot}$, r, and ε).[6]

The power ratio r and the decay constant ε vary from location to location, and we treat them as stochastic variables. The decay constants are modeled as lognormal variates [10]. We found that the lognormal distribution, denoted by $\varepsilon \sim L_N(\mu_{\varepsilon dB};\ \sigma_{\varepsilon\mathrm{dB}})$, with $\mu_{\varepsilon\mathrm{dB}} = 16.1$ and $\sigma_{\varepsilon\mathrm{dB}} = 1.27$ gives the best agreement with the empirical distribution of our measurements.[7] We also found the power ratios r's to be lognormally distributed, i.e., $r \sim L_N(\mu_{r\mathrm{dB}};\ \sigma_{r\mathrm{dB}})$ with $\mu_{r\mathrm{dB}} = -4$ and $\sigma_{r\mathrm{dB}} = 3$, respectively.[8] The parameters are independent of the distance RX-TX.

By integrating the SSA-PDP of each room over all delay bins, we obtain the total average energy $\overline{G}_{tot}$ within each room. The dependence of $\overline{G}_{tot}$ on the T-R separation is given by a

[4] Here and through all the paper, energies are normalized to the total energy received at 1 *m* distance.

[5] According to the bin's width in the delay domain, we can only resolve the MPC's arriving at differential delay greater than 2 *ns*. Thus, even if more than one path arrives within the bin, we refer to the content of each bin as one MPC.

[6] This is due to the fact that *G*tot is related to *G*1, *r*, and ε, see Sec. IV.

[7] To be more precise, we converted the decay constants to a dB scale with reference value 1 *ns*, i.e., $\varepsilon_{\mathrm{dB}} = 10\log_{10}(\varepsilon/1ns)$, and fitted those logarithmic decay constants to a normal distribution. We found that normal distribution with mean 16.1 and standard deviation 1.27 gave the best fit. In the following, we will abbreviate this by saying that the decay constant is distributed lognormally, $\varepsilon \sim L_N(\mu_{\varepsilon\mathrm{dB}};\ \sigma_{\varepsilon\mathrm{dB}})$ with mean $\mu_{\varepsilon\mathrm{dB}} = 16.1$, $\sigma_{\varepsilon\mathrm{dB}} = 1.27$.

[8] Since the *r*-values are already ratios, their representation on a logarithmic scale is straightforward, $r\mathrm{dB} = 10\log(r)$. Again, the histogram of the r_{dB} can be fitted by a normal distribution, now with mean –4 and standard deviation 3.

Dajana Cassioli†, Student Member, IEEE, Moe Z. Win, Senior Member,IEEE, and Andreas F. Molisch, Senior Member, IEEE

pathloss model. Our proposal does not specify the pathloss, but leaves that as a separate topic – we anticipate several proposals to cover that problem.

Moreover, because of the shadowing phenomenon, the $\overline{G}_{tot}$ varies statistically around the value given by the path loss law. In accordance with the literature, we propose a lognormal distribution [10, 11], the standard deviation of the associated normal random variable equal to 4.3.[9]

IV. RELATIONSHIP BETWEEN PARAMETERS

The SSA-PDP of the channel may be expressed as

$$\overline{g}(\tau) = \sum_{k=1}^{N_{bins}} \overline{G}_k \delta(\tau - \tau_k), \tag{2}$$

where the function $\overline{g}(\tau)$ can be interpreted as the average energy received at a certain receiver position and a delay τ, normalized to the total energy received at one meter distance, and N_{bins} is the total number of bins in the observation window. Assuming an exponential decay starting from the second bin, we have

$$\overline{g}(\tau) = \overline{G}_1 \cdot \delta(\tau - \tau_1) + \sum_{k=2}^{N_{bins}} \overline{G}_2 \cdot \exp[-(\tau_k - \tau_2)/\varepsilon] \cdot \delta(\tau - \tau_k), \tag{3}$$

where ε is the decay constant of the SSA-PDP.

The total average energy received over the observation interval T is

$$\overline{G}_{tot} = \int_0^T \overline{g}(\tau) d\tau = \overline{G}_1 + \sum_{k=2}^{N_{bins}} \overline{G}_2 \exp[-(\tau_k - \tau_2)/\varepsilon]. \tag{4}$$

Summing the geometric series we obtain

$$\overline{G}_{tot} = \overline{G}_1 [1 + rF(\varepsilon)], \tag{5}$$

where $r = \overline{G}_2 / \overline{G}_1$ is the power ratio, and

[9] Again, we are considering the logarithm of the path-loss, which is already a ratio (of total received energies at distances of *d* meters and 1 meter), so that the lognormal distribution can be interpreted analogously to the one for *r*.

Dajana Cassioli†, Student Member, IEEE, Moe Z. Win, Senior Member,IEEE, and Andreas F. Molisch, Senior Member, IEEE

$$F(\varepsilon) = \frac{1-\exp[-(N_{bins}-1)\Delta\tau/\varepsilon]}{1-\exp(-\Delta\tau/\varepsilon)} \cong \frac{1}{1-\exp(-\Delta\tau/\varepsilon)}. \quad (6)$$

The total normalized average energy is lognormally distributed, due to the shadowing, around the mean value given from the path loss model *PL*:

$$\overline{G}_{tot} \sim L_N(-PL; 4.3). \quad (7)$$

Inverting (5) we obtain the average energy gains as

$$\overline{G}_k = \begin{cases} \dfrac{\overline{G}_{tot}}{1+rF(\varepsilon)} & \text{for k = 1} \\ \dfrac{\overline{G}_{tot}}{1+rF(\varepsilon)} re^{-\frac{(\tau_k-\tau_2)}{\varepsilon}} & \text{for k = 2,..., N}_{\text{bins}} \end{cases} \quad (8)$$

and (2) may be rewritten as

$$\overline{g}(\tau) = \frac{\overline{G}_{tot}}{1+rF(\varepsilon)} \left\{ \delta(\tau-\tau_1) + \sum_{k=2}^{N_{bins}} \left[re^{-\frac{(\tau_k-\tau_2)}{\varepsilon}} \right] \delta(\tau-\tau_k) \right\}. \quad (9)$$

V. SMALL-SCALE STATISTICS

The differences between the PDPs at the different points within a room (over a finely-spaced measurement grid) are caused by the small-scale fading. In "narrowband" models, it is usually assumed that the magnitude of the first (quasi-LOS) multipath component follows Rician or Nakagami statistics and the later components are assumed to have Rayleigh statistics [12]. However, in UWB propagation each resolved MPC is due to a small number of scatterers, and the amplitude distribution in *each* delay bin differs markedly from the Rayleigh distribution.

In fact, we found that the best-fit distribution of the small-scale magnitude statistics is the Nakagami distribution [13], corresponding to a Gamma distribution of the energy gains. This distribution has been used to model the magnitude statistics in mobile radio when the conditions of the central limit theorem are not fulfilled [14].

Dajana Cassioli†, Student Member, IEEE, Moe Z. Win, Senior Member,IEEE, and Andreas F. Molisch, Senior Member, IEEE

The variations over the measurement grid are treated as stochastic. Let us denote with $\Gamma(\Omega, m)$ the Gamma distribution with parameters Ω and m. The parameters of the Gamma distribution vary from bin to bin: $\Gamma(\Omega_k, m_k)$ denotes the Gamma distribution that describes the energy gains of the local PDPs in the k^{th} bin within each room. The Ω_k are given as $\Omega_k = \overline{G}_k$, i.e., the magnitude of the SSA-PDP in the k^{th} bin. The m_k are related to the variance of the energy gain of the k^{th} bin, and decrease with the increasing excess delay.

The m_k parameters of the Gamma distributions themselves are random variables distributed according to a truncated Gaussian distribution, denoted by $m \sim T_N(\mu_m, \sigma_m^2)$, i.e., their distribution looks like a Gaussian for $m \geq 0.5$ and zero elsewhere:

$$f_m(x) = \begin{cases} K_m e^{-\frac{(x-\mu_m)^2}{2\sigma_m^2}}, & \text{if } x \geq 0.5 \\ 0, & \textit{otherwise} \end{cases} \tag{10}$$

where the normalization constant K_m is chosen so that the integral over the $f_m(x)$ is unity. Mean and variance are given as

$$\mu_m(\tau_k) = 3.5 - \frac{\tau_k}{73}, \tag{11}$$

$$\sigma_m^2(\tau_k) = 1.84 - \frac{\tau_k}{160}, \tag{12}$$

where the unit of τ_k is in nanoseconds.

Finally, the phases of the impulse response in the delay bins are correlated as uniformly distributed random variables (between 0 and 2π). For pure baseband pulses, the model specifies equally likely positive or negative amplitudes.

VI. IMPLEMENTATION RECIPE

In our model the local PDP is fully characterized by the pairs $\{G_k, \tau_k\}$, where $\tau_k = (k - 1)\,\Delta\tau$ with $\Delta\tau = 2$ns. The G_k are generated by a superposition of large and small scale statistics. We start out by generating the total mean energy $\overline{G_{tot}}$ at a certain distance according to (7). Next, we generate the decay constant ε and the power ratio r as lognormal distributed random numbers

Dajana Cassioli†, Student Member, IEEE, Moe Z. Win, Senior Member,IEEE, and Andreas F. Molisch, Senior Member, IEEE

$$\varepsilon \sim L_N(16.1;\ 1.27), \tag{13}$$

$$r \sim L_N(\text{-}4;\ 3)\,. \tag{14}$$

We set the width of the observation window to be $T = 5\varepsilon$. Thus, the SSA-PDP is completely specified according to (9). Finally, we generate the local PDPs by computing the normalized energy gains $G_k^{(i)}$ of every bin k and every location i as Gamma distributed independent variables. The Gamma distributions have the average given by (8), and the m_k's are generated as independent truncated Gaussian random variables

$$m_k \sim T_N(\mu_m(\tau_k); \sigma_m^2(\tau_k)) \tag{15}$$

with $\mu_m(\tau_k)$ and $\sigma_m^2(\tau_k)$ given by (11) and (12).

The computer implementation is summarized in the flowchart of Fig. 1; the statistical models and required parameters are shown in Table II. Small changes in the receiver position result in different local PDPs, corresponding to different realizations of the local energy gains G_k's, whereas the SSA-PDP does not change. When the changes of the receiver position are such that the environment changes as well, the SSA-PDP should be generated according to the new large scale conditions, and the local PDPs are generated about the new SSA-PDP.

TABLE II

GLOBAL PARAMETERS $\Rightarrow$ $\overline{G_{tot}}$ and G_k	
Path Loss	to be determined from other models

Dajana Cassioli†, Student Member, IEEE, Moe Z. Win, Senior Member,IEEE, and Andreas F. Molisch, Senior Member, IEEE

Shadowing	$\overline{G_{tot}} \sim L_N$ (-PL; 4.3)
Decay Constant	$\varepsilon \sim L_N$ (16.1; 1.27)
Power Ratio	$r \sim L_N$ (-4; 3)
LOCAL PARAMETERS $\Rightarrow G_k$	
Energy Gains	$G_k \sim \Gamma(\overline{G}_k; m_k)$
m values	$m_k \sim T_N(\mu_m(\tau_k); \sigma_m^2(\tau_k))$ $\mu_m(\tau_k) = 3.5 - \frac{\tau_k}{73}$ $\sigma_m^2(\tau_k) = 1.84 - \frac{\tau_k}{160}$

VII. CONCLUSIONS

We propose a statistical, tapped-delay line model for the fading statistics of UWB indoor channels. This model is based on the analysis of an extensive measurement campaign in a typical office building. Furthermore, the model is flexible and can be adapted to different environments, e.g., residential homes, by adjusting the parameters.

In contrast to narrowband models, the energy statistics due to small-scale effects follow a Gamma distribution for *all* bins, with the *m*-factor decreasing with increasing excess delay. The variations of the large-scale parameters, such as the total averaged energy, decay constant, and ratio of the energies in the first and second bin, can be modeled as stochastic parameters that change, e.g., from room to room.

With this model, accurate performance predictions of UWB spread spectrum systems become feasible. In a recent work [Cassioli et al., ICC 2002], we have used the model to analyze different types of Rake receivers, showing the usefulness of the proposed model.

ACKNOWLEDGMENTS

We wish to acknowledge Larry J. Greenstein, Tom M. Willis, Jack H. Winters, and Lawrence A. Shepp for helpful discussions.

Dajana Cassioli†, Student Member, IEEE, Moe Z. Win, Senior Member,IEEE, and Andreas F. Molisch, Senior Member, IEEE

REFERENCES

[1] A. A. Saleh and R. A. Valenzuela, "A statistical model for indoor multipath propagation," *IEEE J. Select. Areas Commun.*, vol. 5, pp. 128–137, Feb. 1987.
[2] T. S. Rappaport, S. Y. Seidel, and K. Takamizawa, "Statistical channel impulse response models for factory an open plan building radio communication system design," *IEEE Trans. Commun.*, vol. 39, pp. 794–807, May 1991.
[3] H. Hashemi, "The indoor radio propagation channel," *Proc. IEEE*, vol. 81, pp. 943–968, July 1993.
[4] H. Hashemi, "Impulse response modeling of indoor radio propagation channels," *IEEE J. Select. Areas Commun.*, vol. 11, no. 7, pp. 967–978, 1993.
[5] M. Z. Win, R. A. Scholtz, and M. A. Barnes, "Ultra -wide bandwidth signal propagation for indoor wireless communications," in *Proc. IEEE Int. Conf. on Commun.*, vol. 1, pp. 56–60, June 1997. Montr´eal, CANADA.
[6] M. Steinbauer and A. F. Molisch, "Directional channel models," in *Flexible Personalized Wireless Communications* (L. M. Correia, ed.), (New York, NY 10158-0012), John Wiley & Sons, Inc., 2001. Chap. 3.2.
[7] H. Lee, B. Han, Y. Shin, and S. Im, "Multipath characteristics of impulse radio channels," in *Proc. 50th Annual Int. Veh. Technol. Conf.*, vol. 3, pp. 2487–2491, 2000. Tokyo, JAPAN.
[8] J. R. Foerster, "The effects of multipath interference on the performance of UWB systems in an indoor wireless channel," in *Proc. IEEE Semiannual Veh. Technol. Conf.*, vol. 2, pp. 1176–1180, May 2001. Rhodos, GREECE.
[9] H. Hashemi, "Simulation of the urban radio propagation channel," *IEEE Trans. on Veh. Technol.*, vol. VT-28, pp. 213–225, Aug. 1979.
[10] L. J. Greenstein, V. Erceg, Y. S. Yeh, and M. V. Clark, "A new path-gain/delay-spread propagation model for digital cellular channels," *IEEE Trans. on Veh. Technol.*, vol. 46, pp. 477–485, May 1997.
[11] V. Erceg, L. J. Greenstein, S. Y. Tjandra, S. R. Parko, A. Gupta, B. Kulic, A. A. Julius, and R. Bianchi, "An empirically based path loss model for wireless channels in suburban environments," *IEEE J. Select. Areas Commun.*, vol. 17, pp. 1205–1211, July 1999.
[12] E. Failli, ed., *Digital land mobile radio. Final report of COST 207*. Luxemburg: Commission of the European Union, 1989.
[13] M. Nakagami, "The *m*-distribution–A general formula of intensity distribution of rapid fading," in *Statistical Method in Radio Wave Propagation* (W. C. Ho.man, ed.), (Oxford, U.K.), pp. 3–36, Pergamon Press, 1960.
[14] W. R. Braun and U. Dersch, "A physical mobile radio channel model," *IEEE Trans. on Veh. Technol.*, vol. 40, pp. 472–482, May 1991.
[15] A. F. Molisch and M. Steinbauer, "Condensed parameters for characterizing wideband mobile radio channels," *Int. J. Wireless Information Networks*, vol. 6, pp. 133–154, 1999.
[16] P. A. Bello, "Characterization of randomly time-variant linear channels," *IEEE Trans. Commun. Sys.*, vol.CS-11, pp. 360–393, Dec. 1963.

Dajana Cassioli†, Student Member, IEEE, Moe Z. Win, Senior Member,IEEE, and Andreas F. Molisch, Senior Member, IEEE

Dajana Cassioli†, Student Member, IEEE, Moe Z. Win, Senior Member,IEEE, and Andreas F. Molisch, Senior Member, IEEE

APPENDIX I. THE UWB PROPAGATION EXPERIMENT

Although the purpose of this document is the modeling of the channel rather than on the experiment itself, for the convenience of the reader, we give a review of the UWB propagation experiment that closely follows [5].

A UWB experiment was performed in a modern laboratory/office building having the floor plan shown in Fig. 2. The measurement technique employed in this measurement campaign is to probe the channel periodically with nanosecond pulses and to record its response using a digital sampling oscilloscope (DSO).

A diagram of the measurement apparatus is shown in Fig. 3. The UWB antennas, which are flat and roughly the size of a playing card, display nearly circularly symmetric patterns about their vertical axes. One of the three UWB antennas is set in close proximity to the transmit antenna to supply a trigger signal to the DSO over a long fixed length coaxial cable. Therefore, all recorded multipath profiles have the same absolute delay reference, and time delay measurements of the signals arriving to the receiving antenna via different propagation paths can be made. During each of the multipath profile measurements, both the transmitter and receiver are kept stationary.

The transmitted waveform, measured by the receiving antenna placed 1m away from the transmitting antenna with the same height, is shown in Fig. 4. The repetition rate of the pulses is $2x10^6$ pulses per second, implying that multipath spreads up to 500 *ns* could have been observed unambiguously. Multipath profiles with a duration of 300 *ns* were measured (Fig. 5). Multipath profiles were measured at various locations (see Fig. 2) in 14 rooms and hallways on one floor of the building. Each of the rooms is labeled alpha-numerically. Walls around offices are framed with metal studs and covered with plaster board. The wall around the laboratory is made from acoustically silenced heavy cement block. There are steel core support pillars throughout the building, notably along the outside wall and two within the laboratory itself. The shield room's walls and door are metallic. The transmitter is kept stationary in the central location of the building near a computer server in a laboratory denoted by F. The transmit antenna is located 165 cm from the floor and 105 cm from the ceiling.

In each receiver location, impulse response measurements were made at 49 measurement points, arranged in a fixed-height, 7 x 7 square grid with 15 cm spacing, covering 90cm x 90cm. A total of 741 different impulse responses were recorded. One side of the grid is always parallel to north wall of the room. The receiving antenna is located 120 cm from the floor and 150 cm from the ceiling.

Profiles measured over in offices U, W, and M are shown in Fig. 5. The approximate distances between the transmitter and the locations of these measurements are 10, 8.5, and 13.5 meters respectively. Figure 5 also shows that the response to the first probing pulse has decayed almost completely in roughly 200 *ns*, and has disappeared before the response to the next pulse arrives at the antenna. The multipath profiles recorded in the offices W and M have a substantially lower noise floor than those recorded in office U. This can be explained, with the

Dajana Cassioli†, Student Member, IEEE, Moe Z. Win, Senior Member,IEEE, and Andreas F. Molisch, Senior Member, IEEE

help of Fig. 2, by observing that Office U is situated at the edge of the building with a large glass window and is subject to more external interference (e.g. from radio stations, television stations, cellular and paging towers), while Offices W and M are situated roughly in the middle of the building. In general, an increased noise floor was observed for all the measurements made in offices located at edges of the building with large glass windows.

APPENDIX II. DATA PROCESSING AND ANALYSIS RESULTS

We processed all the multipath profiles measured in the 14 rooms and obtained 14×49 different power delay profiles (PDPs). We separately analyze the effects of the *large* and *small* scale fading statistics. The large scale fading characterizes the changes in the received signal when the receiver position varies over a significant fraction of the transmitter - receiver (T-R) distance and/or the environment around the receiver changes. This situation typically occurs when the receiver is moved from one room to another room in a building.[3] The small-scale effects, on the other hand, are manifested in the changes of the PDP caused by small changes of the receiver position, while the environment around the receiver does not change significantly. This occurs, for instance, when the receiver is moved over the measurement grid within a single room in a building.

In the following, we refer to the PDP measured at one of the 14x49 locations as *local* PDP, while we denote the PDP averaged over the 49 locations within one room as the *small-scale averaged* PDP (SSA-PDP). This spatial averaging (mostly) removes the effect of small scale fading.

The small scale statistics are derived by considering the deviations of the 49 local PDPs from the respective SSA-PDP. The large scale fading may be investigated by considering the variation of the SSA-PDPs over the different rooms. We also make a distinction between the "local" parameters, which refer to the small scale effects, and the "global" parameters, extracted from the SSA-PDPs. For clarity, all the symbols and parameters are listed in Table I.

Since the absolute propagation delays of the received signals vary from one location to another, an appropriate delay reference is needed to characterize the relative delays of each resolved MPC. We take the reference τ_{Ref} as the absolute propagation delay, i.e., the delay of the direct or quasi line-of-sight (LOS) path given according to the geometry: $\tau_{Ref} = d/c$, where d is the T-R separation distance and c is the speed of light. We then translate the delay axis of the measured multipath profiles for each location by its respective τ_{Ref}.

As in [2], the delay axis is quantized into bins, and the received power is integrated within each bin to obtain the local PDP in terms of the pairs $\{G_k, \tau_k\}$, where G_k is the energy gain defined as the ratio between the energy received at a T-R distance d, over a bin width $\Delta\tau$

[3] There could also be large-scale changes within one room if it is large enough. However, with our measurement setup and choice of measurement points, this effect could not be observed. It is also possible that some of the 49 measurement points within one room were shadowed. However, it was not possible to separate this effect from the small-scale fading (see also Sec. 5).

Dajana Cassioli†, Student Member, IEEE, Moe Z. Win, Senior Member,IEEE, and Andreas F. Molisch, Senior Member, IEEE

beginning at the delay $\tau_k = (k-1)\,\Delta\tau$, and the total energy received at the reference distance of one meter.[4]

We chose the widths of the bins to be $\Delta\tau = 2$ ns. This value is a good compromise between high delay resolution, and reduction of the effects of noise and imperfect back-to-back calibration.

To reduce the noise we set the power of all the bins below a threshold to 0. The threshold was set to be 6 dB [15] above the noise floor, which is defined as the average noise energy within one delay bin. The noise floor for each room is computed separately, namely by computing the energies per bin from the portion of the PDP that is measured *before* the first multipath component arrives (i.e., before τ_{Ref}), and averaging these energies over the 49 locations within a room.

A. The Large Scale Statistics

All SSA-PDPs exhibit an exponential decay as a function of the excess delay. Since we perform a delay axis translation, the direct path always falls in the first bin in all the PDPs.[5] It also turns out that the direct path was always the strongest path in the 14 SSA-PDPs even if the line-of-sight is obstructed. The energy of the subsequent MPCs decay exponentially with delay starting from the second bin. This is illustrated by the fit (linearly on a dB scale) in Fig. 6 using the SSA-PDP of a typical high SNR room.

Let $\overline{G}_k = \mathrm{A}_{\mathrm{Spa}}\{G_k\}$ be the locally averaged energy gain, where the $\mathrm{A}_{\mathrm{Spa}}\{\cdot\}$ denotes the spatial average over the 49 locations of the measurement grid. The average energy of the second MPC may be expressed as a fraction r of the average energy of the direct path, i.e. $r = \overline{G}_2/\overline{G}_1$. We refer to r as the *power ratio*. As we will show in Sec. IV, the SSAPDP is completely characterized by $\overline{G}_1$, the power ratio r, and the decay constant ε (or equivalently, by the total average received energy $\overline{G}_{tot}$, r, and ε).[6] The number of resolved MPCs is given by the number of the MPCs that exceed the threshold discussed above and thus, given the threshold, it depends on the shape of the SSA-PDP, characterized by the parameters $\overline{G}_1$, r, and ε. We performed best-fit procedures to extract the ε's and the r's from the SSA-PDP of each room.

The power ratio r and the decay constant ε vary from location to location, and we treat them as stochastic variables. As only 14 values for ε and r were available, it was not possible to extract the *shape* of their distribution from the measurement data. Instead, we assumed a model *a priori* and fitted the *parameters* of this distribution. Previous narrowband studies showed that the

[4] Here and through all the paper, energies are normalized to the total energy received at 1 *m* distance.

[5] According to the bin's width in the delay domain, we can only resolve the MPC's arriving at differential delay greater than 2 *ns*. Thus, even if more than one path arrives within the bin, we refer to the content of each bin as one MPC.

[6] This is due to the fact that Gtot is related to G1, r, and ε, see Sec. IV.

Dajana Cassioli†, Student Member, IEEE, Moe Z. Win, Senior Member,IEEE, and Andreas F. Molisch, Senior Member, IEEE

decay constants are well modeled as lognormal variates [10]. We found that the lognormal distribution, denoted by $\varepsilon \sim L_N(\mu_{\varepsilon dB}; \sigma_{\varepsilon dB})$, with $\mu_{\varepsilon dB} = 16.1$ and $\sigma_{\varepsilon dB} = 1.27$ gives the best agreement with the empirical distribution.[7] The histograms of the experimental decay constants and the theoretically-fitted distribution are shown in Fig. 7. Applying the same procedure to characterize the power ratios r's, we found that they are also lognormally distributed, i.e., $r \sim L_N(\mu_{r dB}; \sigma_{r dB})$ with $\mu_{r dB} = -4$ and $\sigma_{r dB} = 3$, respectively.[8]

We also investigated the possible correlation of the decay constant with the T-R separation, by applying a linear regression to the ε's versus the distance. As Fig. 8 shows, the regression fit of the decay constants ε's decreases with the increasing distance so slightly that we can conclude that it is *de facto* independent.

By integrating the SSA-PDP of each room over all delay bins, we obtained the total average energy $\overline{G}_{tot}$ within each room. We then analyzed its dependence on the T-R separation. As suggested by the scatter plot of Fig. 9, we adopt a breakpoint model, commonly referred to as *dual slope* model, for path-loss *PL* as a function of the distance.
The regression lines are shown in Fig. 9 and the parameters extracted by performing a best-fit of the empirical attenuation are:

$$PL = \begin{cases} 20.4 \cdot \log_{10}(d/d_0), d = 11m \\ -56 + 74 \cdot \log_{10}(d/d_0), d > 11m \end{cases} \quad \text{(A1)}$$

where *PL* is expressed in dB, d_0=1 m is the reference distance and d is the T-R separation distance in meters. Because of the shadowing phenomenon, the $\overline{G}_{tot}$ varies statistically around the value given by (A1). A common model for shadowing is lognormal distribution [10, 11]. By assuming such model, we found that $\overline{G}_{tot}$ is lognormally distributed about (A1) with a standard deviation of the associated normal random variable equal to 4.3.[9]

B. The Small Scale Statistics

[7] To be more precise, we converted the decay constants to a dB scale with reference value 1 *ns*, i.e., $\varepsilon_{dB} = 10 \log_{10}(\varepsilon/1ns)$, and fitted those logarithmic decay constants to a normal distribution. We found that normal distribution with mean 16.1 and standard deviation 1.27 gave the best fit. In the following, we will abbreviate this by saying that the decay constant is distributed lognormally, $\varepsilon \sim L_N(\mu_{\varepsilon dB}; \sigma_{\varepsilon dB})$ with mean $\mu_{\varepsilon dB} = 16.1$, $\sigma_{\varepsilon dB} = 1.27$.

[8] Since the r-values are already ratios, their representation on a logarithmic scale is straightforward, rdB =10 log(r). Again, the histogram of the r_{dB} can be fitted by a normal distribution, now with mean –4 and standard deviation 3.

[9] Again, we are considering the logarithm of the path-loss, which is already a ratio (of total received energies at distances of d meters and 1 meter), so that the lognormal distribution can be interpreted analogously to the one for r.

Dajana Cassioli†, Student Member, IEEE, Moe Z. Win, Senior Member,IEEE, and Andreas F. Molisch, Senior Member, IEEE

The differences between the PDPs at the different points of the measurement grid are caused by the small-scale fading. In "narrowband" models, it is usually assumed that the magnitude of the first (quasi-LOS) multipath component follows Rician or Nakagami statistics and the later components are assumed to have Rayleigh statistics [12]. However, in UWB propagation each resolved MPC is due to a small number of scatterers, and the amplitude distribution in *each* delay bin differs markedly from the Rayleigh distribution.

In fact, the presented analysis showed that the best-fit distribution of the small-scale magnitude statistics is the Nakagami distribution [13], corresponding to a Gamma distribution of the energy gains. This distribution has been used to model the magnitude statistics in mobile radio when the conditions of the central limit theorem are not fulfilled [14].

We characterize the small scale statistics by fitting the received normalized energies $\{G_k^{(i)}\}$ in *each* bin at the 49 locations of the measurement grid to a distribution.[10]

The variations over the measurement grid are treated as stochastic. The result shows that the statistics of the energy gain vary with delays. Let us denote with $\Gamma(\Omega, m)$ the Gamma distribution with parameters Ω and m. The $\Gamma(\Omega, m)$ gives a good fit of the empirical distribution of the energy gains. The accuracy of the fit has been quantified in terms of the relative mean squared error, which varies between 0.0105 (for the highest SNR) to 0.1137 (for the lowest SNR). A comparison between experimental and theoretical histograms for one exemplary bin in a typical high-SNR is shown in Fig. 10.

The parameters of the Gamma distribution vary from bin to bin: $\Gamma(\Omega_k, m_k)$ denotes the Gamma distribution that fits the energy gains of the local PDPs in the k^{th} bin within each room. The Ω_k are given as $\Omega_k = \overline{G}_k$, i.e., the magnitude of the SSA-PDP in the k^{th} bin. The m_k are related to the variance of the energy gain of the k^{th} bin. Figure 11 shows the scatter plot of the m_k as a function of excess delay for all the bins (except the line-of-sight components). It can be seen from Fig. 11 that the m_k values range between 1 and 6 (rarely 0.5), decreasing with the increasing excess delay. This implies that MPCs arriving with large excess delays are more diffused than the first arriving components, which agrees with intuition.

The m_k parameters of the Gamma distributions themselves are random variables distributed according to a truncated Gaussian distribution, denoted by $m \sim T_N(\mu_m, \sigma_m^2)$, i.e., their distribution looks like a Gaussian for $m \geq 0.5$ and zero elsewhere:

$$f_m(x) = \begin{cases} K_m e^{-\frac{(x-\mu_m)^2}{2\sigma_m^2}}, & \text{if } x \geq 0.5 \\ 0, & \textit{otherwise} \end{cases} \qquad \text{(A2)}$$

where the normalization constant K_m is chosen so that the integral over the $f_m(x)$ is unity.

[10] In the notation $G_k^{(i)}$ the subscript k indicates the k^{th} bin at delay τ_k, while the superscript i indicates the i^{th} location on the grid.

Dajana Cassioli†, Student Member, IEEE, Moe Z. Win, Senior Member,IEEE, and Andreas F. Molisch, Senior Member, IEEE

Figure 12 shows the mean and variance of such Gaussian distributions that fits m_k as a function of the excess delay, along with the respective regression lines. The regression lines are given by

$$\mu_m(\tau_k) = 3.5 - \frac{\tau_k}{73}, \tag{A3}$$

$$\sigma_m^2(\tau_k) = 1.84 - \frac{\tau_k}{160}, \tag{A4}$$

where the unit of τ_k is in nanoseconds.

C. Correlation of MPCs Among Different Delay Bins

We next evaluate the correlation between the energy gain of the MPCs arriving in the same room at different excess delays as

$$\rho_{k,k+m} = \frac{\mathrm{A}_{Spa}\left\{\left(G_k - \overline{G_k}\right)\left(G_{k+m} - \overline{G_{k+m}}\right)\right\}}{\sqrt{\mathrm{A}_{Spa}\left\{\left(G_k - \overline{G_k}\right)^2\right\}\mathrm{A}_{Spa}\left\{\left(G_{k+m} - \overline{G_{k+m}}\right)^2\right\}}}.$$

The analysis shows that the correlation coefficients remain below 0.2 for almost all rooms and delay bins, and is thus negligible for all practical purposes. This allows important conclusions about the propagation mechanisms. Correlation could come from three effects:
(i) each scatterer could induce "wavelength dispersion" by having strongly frequency dependent reflection/diffraction properties in the considered band
(ii) the delay of a scatterer could lie at the boundary of two adjacent bins even after the time-of-arrival shift described above, or
(iii) the uncorrelated scattering (US) assumption [16] could be violated.
Since the correlation coefficients are very small, we conclude that none of those three effects has a marked impact.

We summarize our findings of the data analysis as follows. The average energy gains $\overline{G_k}$ vary both with the excess delay and the large scale conditions, while the m_k parameters depend only on the excess delay.[11]

[11] Future refinements of the model could include spatial coherence lengths for the $\overline{G_k}$'s and m_k's, as well as a possible distance dependence of the m_k's.

Dajana Cassioli†, Student Member, IEEE, Moe Z. Win, Senior Member,IEEE, and Andreas F. Molisch, Senior Member, IEEE

Given the $\overline{G_k}$ and the m_k, the normalized energy gain of the MPCs arriving in the same room at different excess delays are independent realizations of the gamma distribution Γ ($\overline{G_k}$; m_k).

Dajana Cassioli†, Student Member, IEEE, Moe Z. Win, Senior Member,IEEE, and Andreas F. Molisch, Senior Member, IEEE

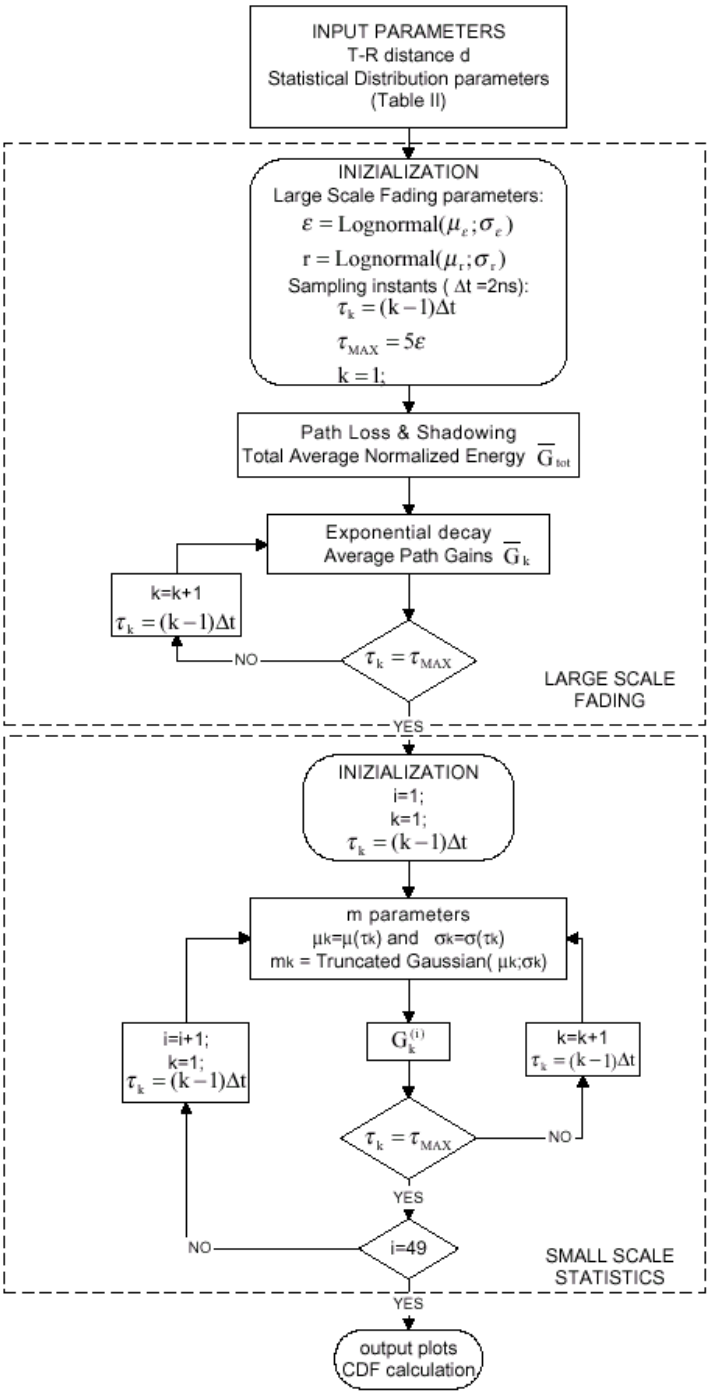

Fig.1. The flowchart of the simulation procedure.

Dajana Cassioli†, Student Member, IEEE, Moe Z. Win, Senior Member,IEEE, and Andreas F. Molisch, Senior Member, IEEE

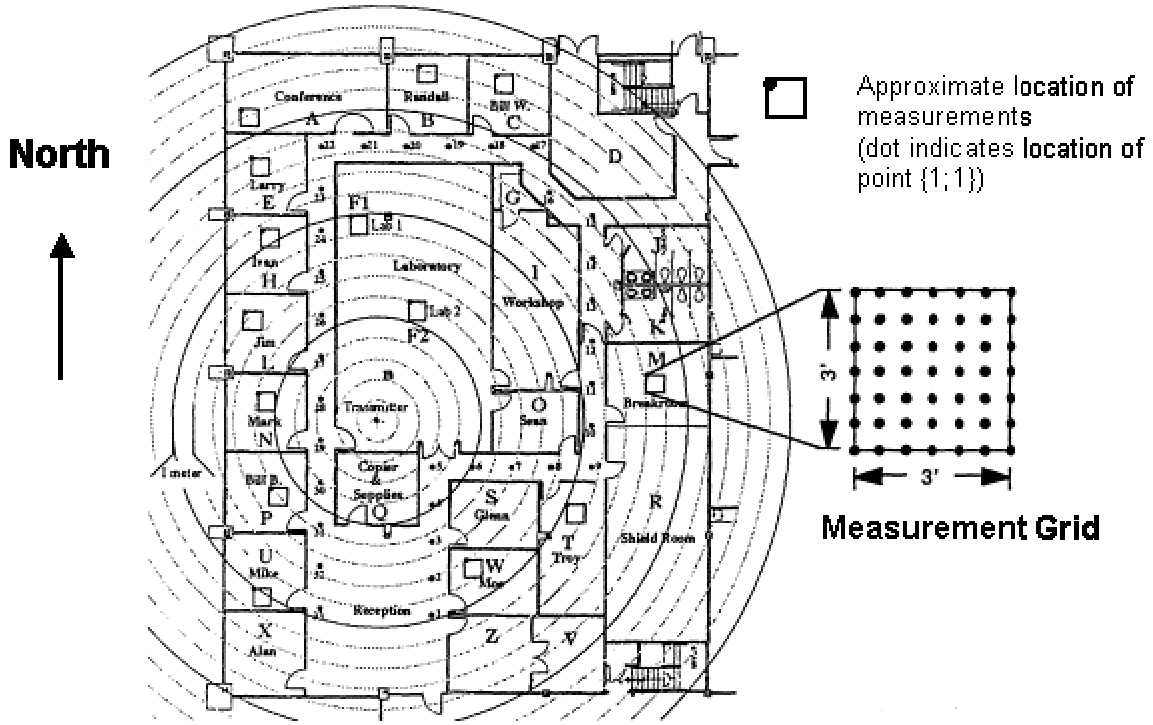

Fig.2. The floor plan of a typical modern office building where the propagation measurement experiment was performed. The concentric circles are centered on the transmit antenna and are spaced at 1 meter intervals.

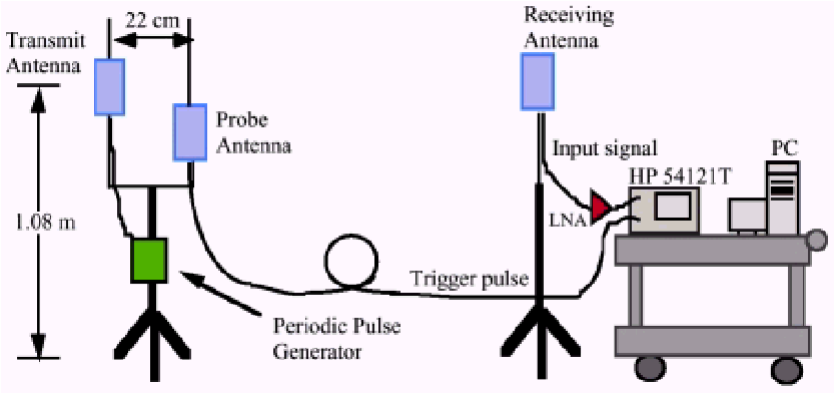

Fig.3. A block diagram of the measurement apparatus.

Dajana Cassioli†, Student Member, IEEE, Moe Z. Win, Senior Member,IEEE, and Andreas F. Molisch, Senior Member, IEEE

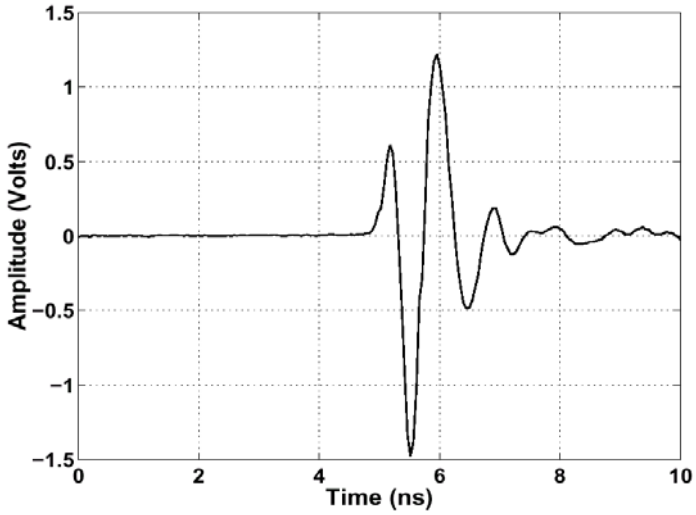

Fig.4. The transmitted pulse measured by the receiving antenna located 1m away from the transmitting antenna with the same height.

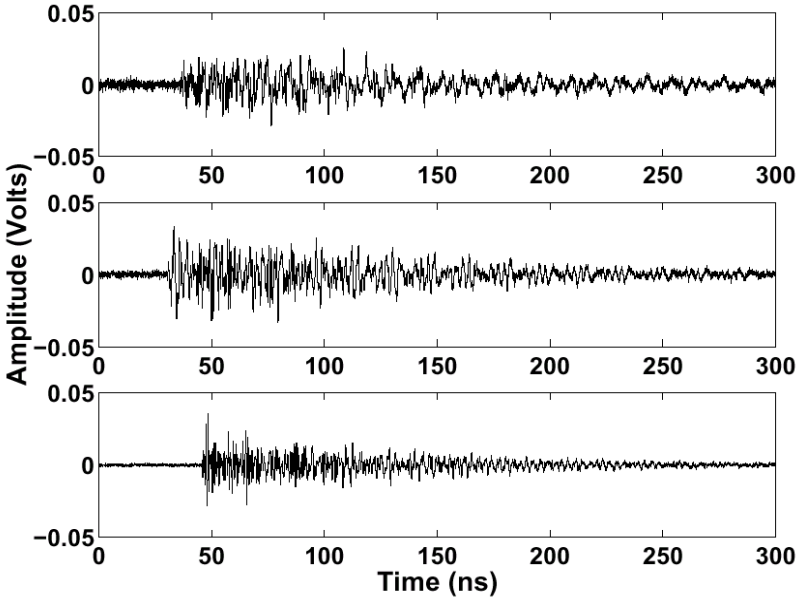

Fig.5. Average multipath measurements of 32 sequentially measured multipath profiles where the receiver is located at the same exact locations in offices U (upper trace),W(middle trace),and M (lower trace). The measurement grids are 10,8.5,and 13.5 meters away from the transmitter respectively.

Dajana Cassioli†, Student Member, IEEE, Moe Z. Win, Senior Member,IEEE, and Andreas F. Molisch, Senior Member, IEEE

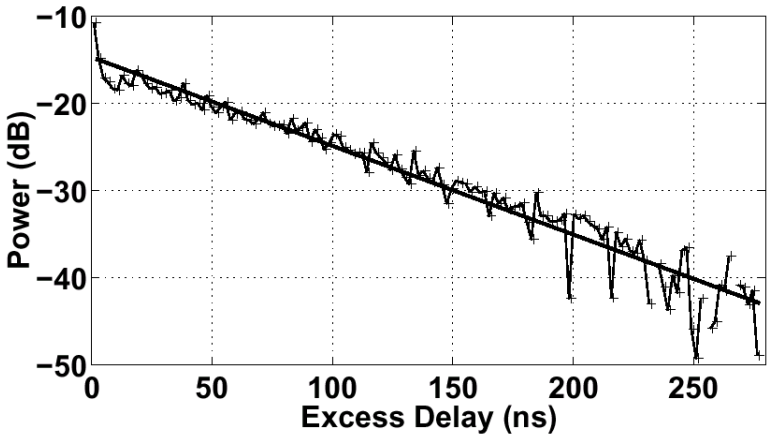

Fig.6. The average power delay profile versus the excess delay in a semi-logarithmic scale for a typical high SNR room. The wavy line is the measured profile, the straight line is the exponential decay obtained by a best fit procedure.

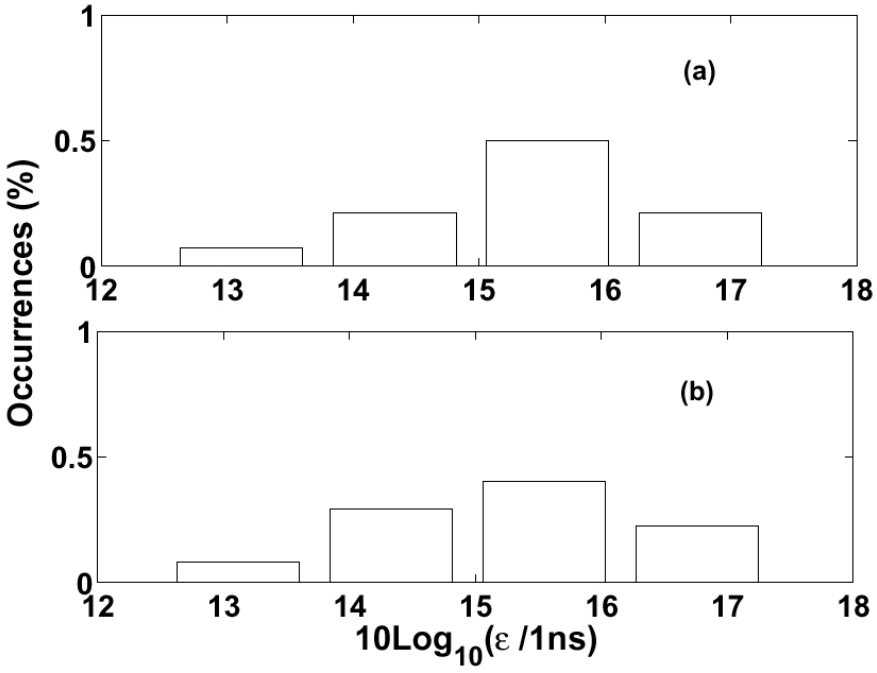

Fig.7. Histograms of the experimental decay constants ε (a) and of the theoretically-fitted distribution (b). The decay constants are expressed in logarithmic units by referring to nanoseconds.

Dajana Cassioli†, Student Member, IEEE, Moe Z. Win, Senior Member,IEEE, and Andreas F. Molisch, Senior Member, IEEE

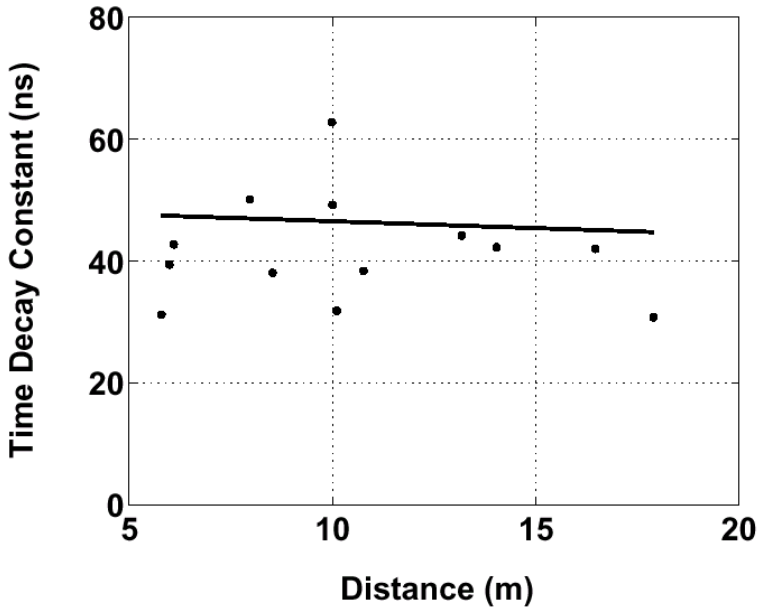

Fig.8. Scatter plot of the decay constants ε versus the T-R distance. The solid line is the regression fit whose slope is -0 .22ns/m.

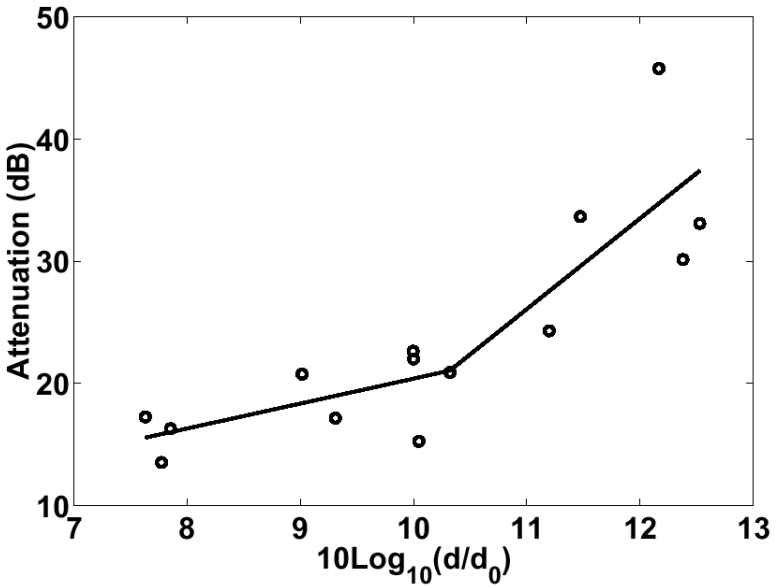

Fig.9. Scatter plot of the large scale attenuation versus the logarithm of the distance. The solid line represents the best-fit with the path loss model of (1).

Dajana Cassioli†, Student Member, IEEE, Moe Z. Win, Senior Member,IEEE, and Andreas F. Molisch, Senior Member, IEEE

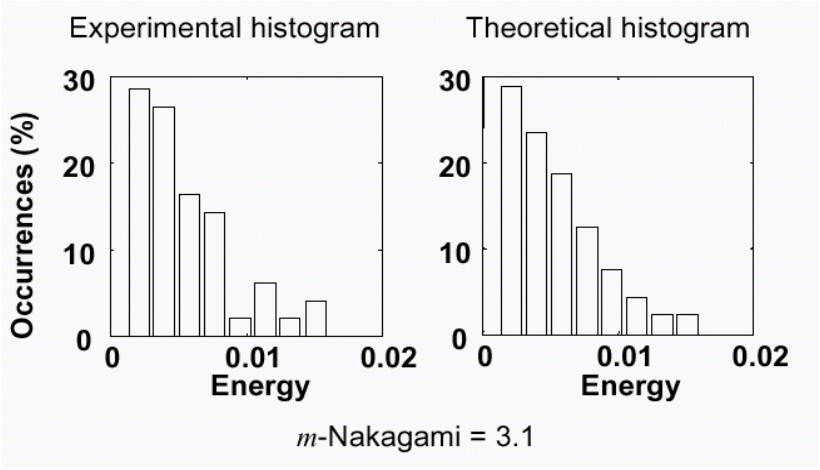

Fig.10. Histogram of the receive energy in the 34 th bin of a typical high SNR room,compared with the theoretical Gamma distribution,whose mean Ω34 and m 34 were extracted from the experimental PDP. The energies on the horizontal axes are expressed in arbitrary units.

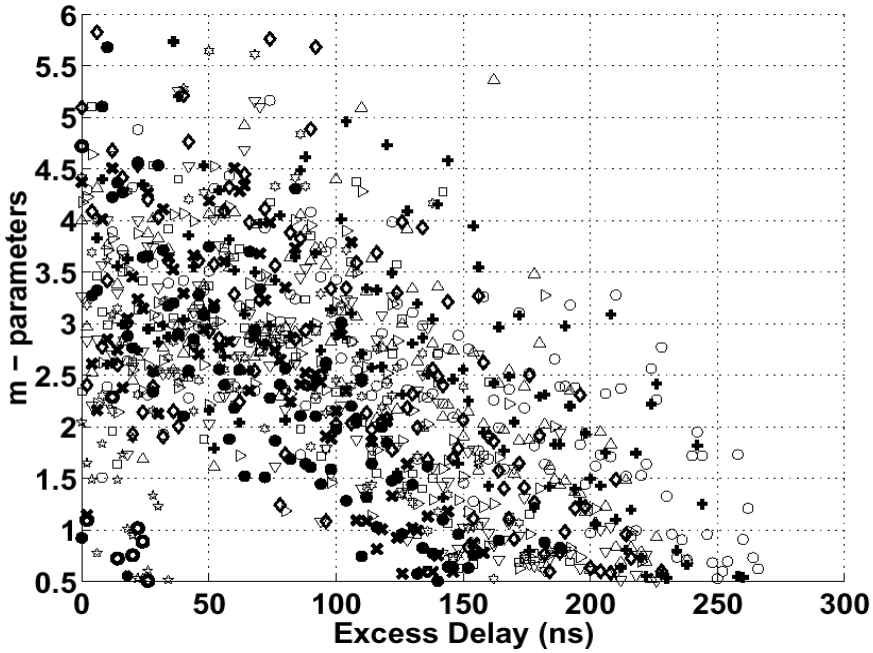

Fig.11. Scatter plot of the *m*-Nakagami parameters of the best fit distribution versus excess delay for all the bins except the line-of-sight components. Different markers correspond to measurements in different rooms.

Dajana Cassioli†, Student Member, IEEE, Moe Z. Win, Senior Member,IEEE, and Andreas F. Molisch, Senior Member, IEEE

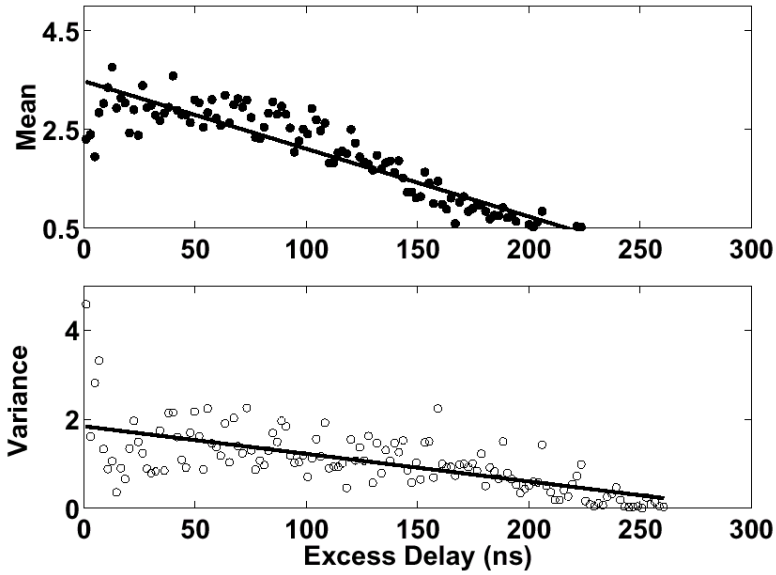

Fig.12. Scatter plot of the mean values (dots)and the variance (circles)of the Gaussian distributions that fit the experimental distribution of m values at each excess delay. The solid lines represent the linear regression for these parameters, respectively.

Dajana Cassioli†, Student Member, IEEE, Moe Z. Win, Senior Member,IEEE, and Andreas F. Molisch, Senior Member, IEEE